



Effect of synthesis method on photocatalytic activity of Ag_3PO_4 evaluated by different dyes

A. El Yacoubi¹, A. Rezzouk², B. Sallek³, B. Chafik El Idrissi¹

1. Chemical Team Materials Surfaces Interfaces, Laboratory Materials and Energitics, Fac of Sciences, University Ibn Tofail, kenitra, B.P: 133, Kénitra, Morocco

2. LPS, Fac. des Sciences Dhar El Mehraz, BP 1796, Atlas FES, Morocco.

3. Laboratoire d'Agroressources et Génie des Procédés, Faculté des Sciences, Université Ibn Tofail, B.P: 133, Kénitra, Morocco

Received 22 Jun 2017,
Revised 21 Oct 2017,
Accepted 25 Oct 2017

Keywords

- ✓ Photocatalysis,
- ✓ Ag_3PO_4 ,
- ✓ Pollutants' degradation,
- ✓ Visible light.

chidrissi@yahoo.fr

Phone: +2126 61 61 65 92

Abstract

Silver phosphate as a highly efficient photocatalyst has received great attention in the recent years. The energy band gap situated in the visible range, thus this material is a potential candidate for replacing titania which is photoactive only under UV. The effect of the liquid-liquid (L-L) simple precipitation method, liquid-solid (L-S) mixture precipitation and solid-solid (S-S) mechanical homogenization of powder precursors on the photocatalytic activity of the Ag_3PO_4 photocatalysts was examined. The morphology and structure of the Ag_3PO_4 crystals were investigated by using X-ray powder diffractometry, scanning electron microscopy, and ultraviolet-visible absorption spectroscopy. The photoactivity of the materials was evaluated by their ability to decolorize methylene blue, methyl orange and congo red under visible-light irradiation. The nanorod-dodecahedral Ag_3PO_4 synthesized by liquid-solid method exhibits superior photocatalytic activity for the photodegradation of the three dyes molecules under artificial lighting irradiation, followed by Ag_3PO_4 synthesized by liquid-liquid method.

1. Introduction

Fresh water is a basic commodity needed in ever-increasing quantities by human society. However, many water sources can be contaminated and thus poisoned by organic pollutants from various origins such as industrial effluent and wastewater [1,2]. Semiconductor-based photocatalysis has been widely regarded as a promising technology to solve the problem of energy shortage and environmental deterioration because of its high efficiency, environmental and low cost, especially for application of wastewater treatment [3]. Generally, a good photocatalyst is mainly dependent on visible light absorption and effective separation of the photoinduced electron-hole pairs. Various photocatalysts have been investigated, and titanium dioxide (TiO_2) is the most widely studied [4]. Nevertheless, its large-scale industrial application was severely restricted due to its lack of visible light absorbance, high photoinduced charge recombination rate and difficulty of separation and recycle from the suspending slurry [5]. Therefore, it is necessary to develop novel photocatalysts particularly with visible light response. Silver phosphate (Ag_3PO_4), discovered by Ye and co-workers [6], is a new and efficient photocatalyst with visible light response, it is an active semiconductor in photo-oxidation, high activity with absorbance in the visible light and high charged carrier mobility, and exhibits extremely high degradation efficiency toward organic dyes under visible light irradiation. Zhu et al. investigated the origin of photocatalytic activation of Ag_3PO_4 via first-principle density functional theory, showing that Ag_3PO_4 had a large dispersion of conduction band and the inductive effect of PO_4^{3-} , favoring the separation of electron-hole pairs [7].

Accordingly, the materials can be synthesized by different methods: hydrothermal [8], ion-exchange [9], thermolysis [10] and ultrasound-precipitation process [11]. It is well known that the photocatalytic properties of photocatalysts are greatly affected by the morphology [12], thus many methods have been evolved to synthesize the Ag_3PO_4 catalysts with various morphologies and sizes, which include spheres [13], dodecahedrons [14], tetrahedrons [15], cubes [16, 17] and other Ag_3PO_4 crystals with various new morphologies.

In this work, in order to explore the effect of the types of synthesis on the structure, morphology, and photocatalytic activity of Ag_3PO_4 , we synthesized Ag_3PO_4 samples using liquid-liquid, solid-solid and liquid-

solid methods at room temperature without any surfactant adding, using $(\text{NH}_4)_2\text{HPO}_4$ and AgNO_3 as precursors. The photocatalytic properties were evaluated through the degradation of methylene blue (MB), orange methyl (MO) and congo red (GR) organic dye molecules.

2. Materials and Methods

2.1. Synthesis and characterization

All reagents were analytical grade and used without further purification. The Ag_3PO_4 sample prepared with liquid-liquid method (Ag_3PO_4 L-L) by directly mixing Ag_3PO_4 aqueous solution with $(\text{NH}_4)_2\text{HPO}_4$ solution under dropwise addition followed by vigorous stirring. Typically, 0.408 g AgNO_3 was first dissolved in 20 mL (0.12 M) deionized (DI) water. Then, a uniform $(\text{NH}_4)_2\text{HPO}_4$ aqueous solution (0.04 M) was formed by mixing 0.108 g $(\text{NH}_4)_2\text{HPO}_4$ with 20 mL DI water and was dropwise injected to the above solution under magnetic stirring during 2 h in the dark. In the case of the silver phosphate prepared by solid-solid method (Ag_3PO_4 S-S), $(\text{NH}_4)_2\text{HPO}_4$ and AgNO_3 powders were mixed in a mortar until a yellow paste arised which was subsequently washed with distilled water. Lastly, the Ag_3PO_4 powder is also synthesized through liquid-solid mixture precipitation method (Ag_3PO_4 L-S) with simple addition of AgNO_3 powder on ammonium hydrogen phosphate solution. In other words, 2.4 mmol of the AgNO_3 powder is directly and slowly added to 0.04 M of $(\text{NH}_4)_2\text{HPO}_4$ solution previously prepared at room temperature and then was immediately mixed and vigorously stirred for 2 h in the dark. The as-synthesized yellow precipitates by L-L and L-S reactions were separated by filtration, washed several times with DI water. Finally all the samples were dried at 80°C for 12 h.

Phase and crystal sizes were characterized by an X-ray diffractometer (XRD, Philips X'Pert PRO) using a $\text{CuK}\alpha$ $\lambda = 1.5406 \text{ \AA}$ radiation at 40 kV and 30 mA in the range of $10\text{--}60^\circ$. The morphologies of the photocatalysts were investigated by scanning electronic microscopy.

2.2. Photocatalytic measurements

The photocatalytic activities were investigated through the degradation of the cationic dye MB and the anionic dyes CR and MO in an aqueous under visible light (36W LED lamp). In a typical process, 50 mg of the as-prepared Ag_3PO_4 photocatalysts was dispersed into 50 ml aqueous dye solution (20 mg/l), which were stirred in the dark for 30 min to establish an adsorption-desorption equilibrium of dye on the surface of photocatalyst. The sample was periodically withdrawn, centrifuged to separate the photocatalyst from solution, and used for the absorbance measurement. The absorption spectra of the solutions were determined using a UV–vis spectrophotometer (Jenway, Serial: 67XX) and the decolorization was calculated using the following equation:

$$\text{Decolorization}(\%) = \left(\frac{C}{C_0}\right) \times 100 = \left(\frac{A}{A_0}\right) \times 100 \quad (1)$$

Where C_0 and A_0 are the concentration and absorbance of the dye before irradiation, respectively, and C and A are the corresponding concentration and absorbance of the dye after light irradiation, respectively.

3. Results and discussion

The phase structure and purity of the product were characterized by XRD. Figure 1 shows the XRD patterns of all as-obtained products. All of the diffraction peaks can be indexed to the body-centered cubic structure of Ag_3PO_4 with the space group P4-3n (JCPDS card No.06–0505) [18]. No peaks assignable to other phases were observed; indicating that high purity Ag_3PO_4 was obtained. The sharp and strong diffraction peaks indicate that the Ag_3PO_4 in each product was well crystallized.

The peaks at 20.88, 29.69, 33.30, 36.59, 42.49, 47.81, 52.70, 55.03 and 57.30 correspond to the (1 1 0), (2 0 0), (2 1 0), (2 1 1), (2 2 0), (3 1 0), (2 2 2), (3 2 0) and (3 2 1) planes of the Ag_3PO_4 particles, respectively. Lattice dimensions were calculated for the fitted peaks by using a Fullprof suite software program. The mean crystallite size (L) of the particles was calculated from the XRD line broadening measurement using the Scherrer equation (2) [19]:

$$L = \frac{k\lambda}{\beta \cos \theta} \quad (2)$$

Where L = crystallite size, K = the shape factor equal to 0.9, λ = wavelength of $\text{Cu K}\alpha$ radiation equal to 1.5406 \AA , θ = half of the diffraction angle and β = full width at half maximum (FWHM), the Scherrer equation is relative to a single peak (210). A standard silicon sample was used prior to the application of our samples.

The estimated average crystallite size and lattice parameters were 56 nm and $a = 6.013950\text{\AA}$; 82 nm and $a = 6.011941\text{\AA}$ and 69 nm and $a = 6.013204\text{\AA}$ for Ag_3PO_4 L-L, Ag_3PO_4 L-S and Ag_3PO_4 S-S, respectively. Widely accepted, well crystallinity corresponded to less bulk phase defects. That is, well crystallinity facilitated separation of charge carriers and enhancement of photocatalytic efficiency. Thus, it can be concluded that

Ag_3PO_4 microcrystals should possess high photocatalytic activity. According to the XRD patterns, the intensity ratio of the (110) and (200) facet diffraction peaks for the samples prepared with different methods was 0.72, 0.71 and 0.91 for Ag_3PO_4 L-L, Ag_3PO_4 L-S and Ag_3PO_4 S-S, respectively. This variation in intensity ratio assumes to the change in morphology.

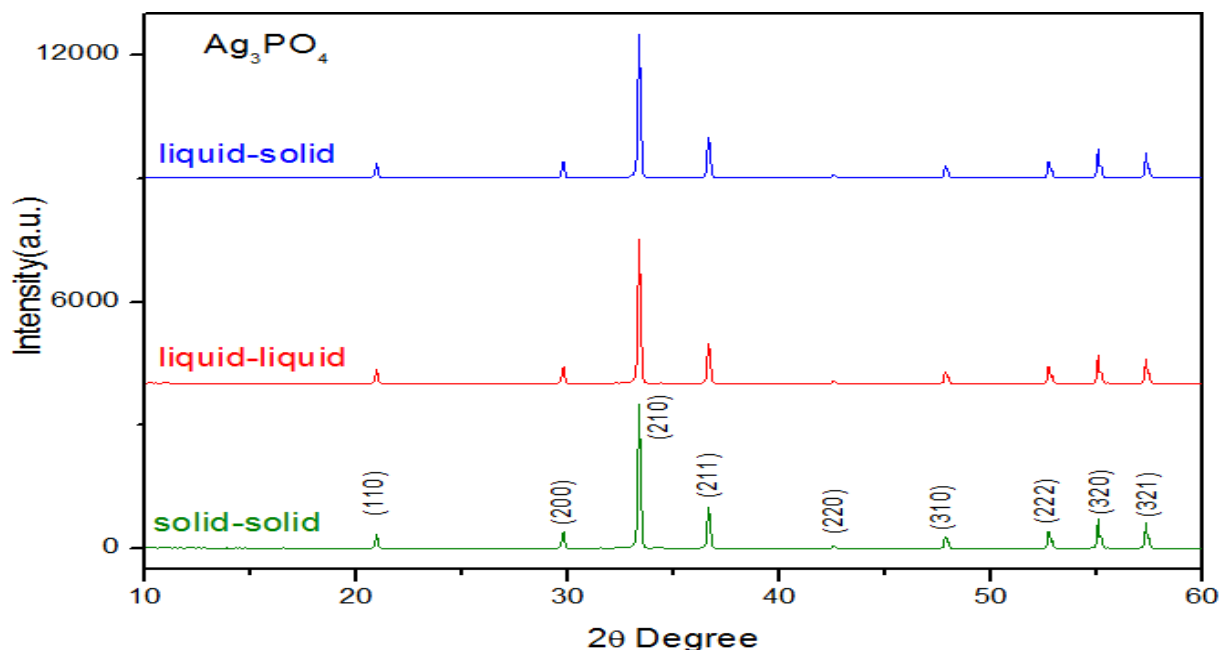


Figure 1: XRD patterns of the Ag_3PO_4 photocatalysts prepared with different methods

The morphological characteristics of the synthesized photocatalysts were examined with SEM, and representative images obtained from the Ag_3PO_4 samples are shown in Fig. 2. It can be found that the three kinds of products are composed of irregular particles with lacking uniformity in both distribution and shape. Fig.2a shows SEM pictures of Ag_3PO_4 L-L, the SEM analyze do not show any regular shape of Ag_3PO_4 particles. It is then necessary to have a better resolution for the analysis of morphology. The particle size is between 280 and 400 nm. Also, some aggregation phenomenon could be observed. The Ag_3PO_4 L-S and Ag_3PO_4 S-S samples exhibited typical morphologies where a mixture of nanorod and irregular polyhedra (Fig. 2b) and irregular dodecahedra (Fig. 2c) can be observed with smooth surfaces, respectively. The particles are varying sizes ranging from 1.5 microns to about 9 in both Ag_3PO_4 L-S and Ag_3PO_4 S-S.

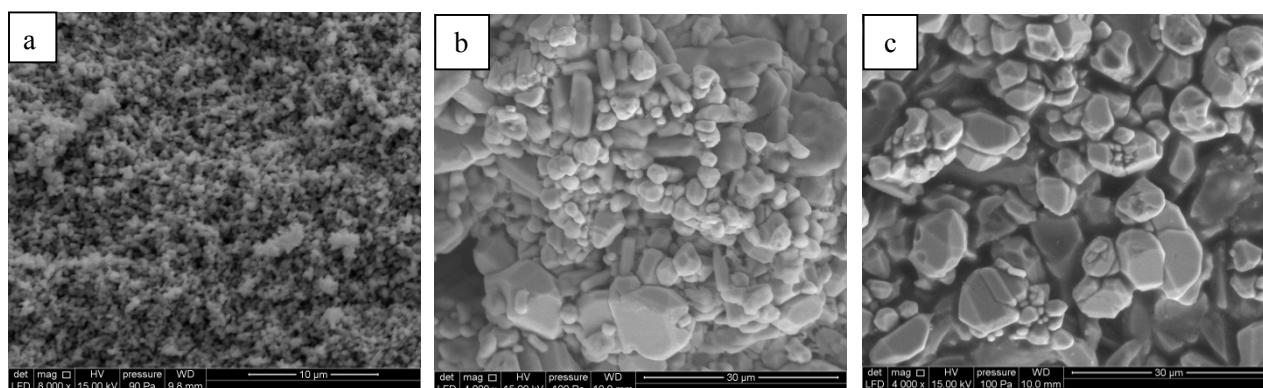


Figure 2 : SEM images of the samples prepared with different methods: (a) Ag_3PO_4 L-L, (b) Ag_3PO_4 L-S and (c) Ag_3PO_4 S-S

Dye effluents from textile industries and photographic industries are becoming a serious environmental problem because of their toxicity, unacceptable color, high chemical oxygen demand content, and resistance to chemical, photochemical, and biological degradation [20]. The photocatalytic performance of Ag_3PO_4 is highly specific to the nature of pollutant [14, 21]. To determine the photocatalytic activities, Ag_3PO_4 L-L, Ag_3PO_4 L-S and Ag_3PO_4 S-S were selected for the degradation of OM, MB, and CR in the dark and under visible light at room temperature.

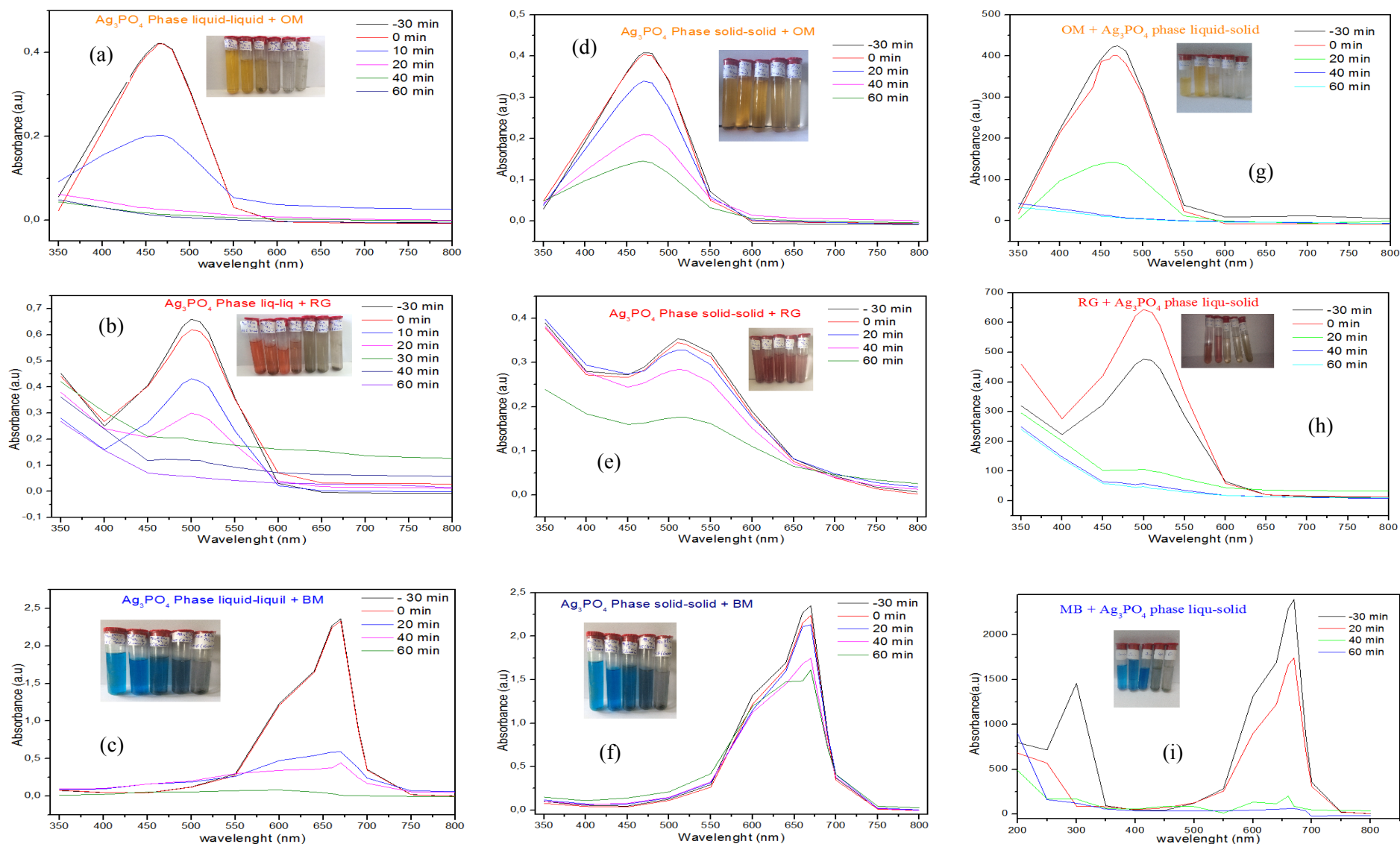


Figure 3: UV-visible absorption of three dyes (OM, RG, BM) photocatalysed by (a-c) Ag_3PO_4 L-L, (d-f) Ag_3PO_4 S-S and (g-i) Ag_3PO_4 L-S

As shown in Fig. 3a-i, the intensity of the OM, MB, and CR absorption peaks (465 nm, 664 nm, and 510 nm, respectively) rapidly decreased under UV-Visible light irradiation and the solutions were decolorized excepted for Ag_3PO_4 S-S (fig.3d-f) photocatalyst where the degradation of the dyes was restricted. The decrease in absorbance of MB solution at 664 nm is usually taken as a reference for evaluating the decolorization rate of this organic dye i.e the destruction of its chromophore. However, the absorbance of MB solution at 291 nm gives information about the degradation stage of the entire dye [22]. The small peak around 200 nm (fig. 3i) increases with increasing irradiation time from 40 to 60 min. This observation indicates that some intermediates with the single aromatic ring are produced accompanying with the quick cleavage of the whole conjugated chromophore structure of MB [23].

The corresponding degradation curves are shown in Fig. 4a-c, in the absence of Ag_3PO_4 Catalyst (blank test), removal of the dyes was almost negligible (data not shown). Before the photocatalytic reaction, the sample suspension was stirred for 30 min in the dark to reach the adsorption-desorption equilibrium, the dark test exhibits a poor activity, which excludes the possibility of photolysis, this might be associated with the active sites such as OH defects on the surface of the catalysts [24, 25] as well as the particle size [26]. After 30 min in the dark condition, the degradation efficiency of all Ag_3PO_4 samples was further increased when it absorbed visible light, demonstrating the three Ag_3PO_4 catalysts showed the photocatalytic properties.

Fig. 4a shows the photocatalytic efficiency curves of Ag_3PO_4 L-S under visible light irradiation for different dyes: MO, CR and MB. The Ag_3PO_4 L-S photocatalyst exhibits very good photocatalytic activity for all dyes photodegradation under visible irradiation, after visible irradiation for 40 min, 97.88, 94.54 and 91.61% of OM, MB and CR is photodegraded, respectively (table 1). Similar phenomena are observed for the photodegradation of the three dyes by Ag_3PO_4 L-L photocatalyst (Fig. 4b), after visible irradiation for 40 min (table 1), 96.68, 81.81 and 81.21% of OM, MB and CR is photodegraded, respectively.

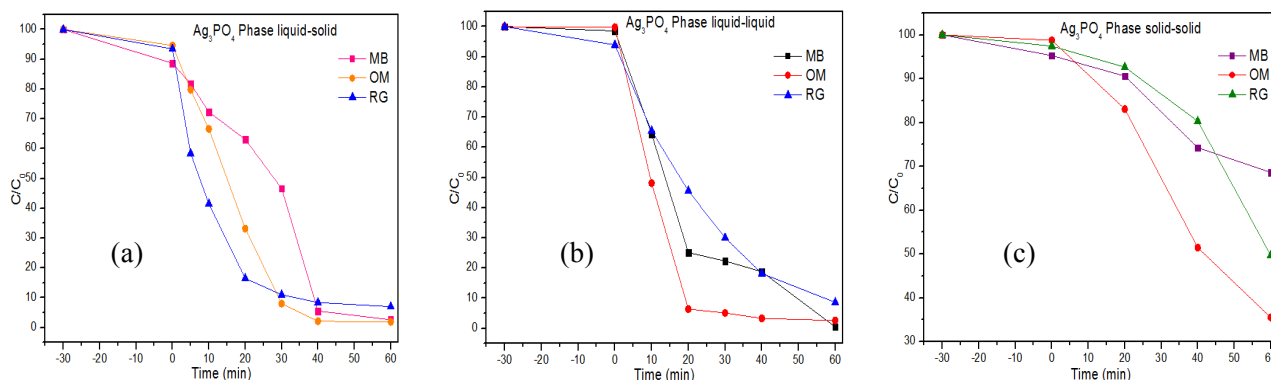


Figure 4: Photocatalytic degradation of OM, MB and CR by the as-prepared photocatalysts (a) Ag_3PO_4 L-S (b) Ag_3PO_4 L-L and (c) Ag_3PO_4 S-S under visible-light irradiation.

On the other hand the maximum discoloration is reached after 60 min of irradiation i.e 97.39, 99.49 and 91.36%. We can see that Ag_3PO_4 L-S photocatalyst exhibited a photocatalytic activity relatively higher than that exhibited by Ag_3PO_4 L-L. From the Fig. 4c it can be seen that Ag_3PO_4 S-S had the smallest adsorption capacity among the three samples and showed different photodegradation performance towards different dyes. Indeed, within 60 min of visible irradiation, only 64.46, 31.36 and 50.28% of OM, MB and CR is photodegraded, respectively.

Table 1: Photocatalytic degradation of different dyes by different Ag_3PO_4 samples

Preparation method	MO degradation rate (%)	CR degradation rate (%)	MB degradation rate (%)
<i>After 40 min under visible light irradiation</i>			
Solid-Solid (S-S)	48.52	19.77	25.71
Liquid-solid (L-S)	97.88	91.61	94.54
Liquid-Liquid (L-L)	96.68	81.21	81.81
<i>After 60 min under visible light irradiation</i>			
Solid-Solid (S-S)	64.46	50.28	31.36
Liquid-solid (L-S)	98.11	93.01	97.41
Liquid-Liquid (L-L)	97.39	91.36	99.49

In summary, the degradation efficiency of OM, MB and CR solutions follows the order: Ag_3PO_4 L-S > Ag_3PO_4 L-L >> Ag_3PO_4 S-S. It is well known that the morphology of materials is closely related to the exposed facets of the crystals, which directly affect the properties of the catalysts [12]. Obviously, the higher photocatalytic activity of Ag_3PO_4 L-S can be explained by the morphology of the silver phosphate particles where Ag_3PO_4 L-S had a mixture of nanorod and irregular polyhedra morphology while Ag_3PO_4 S-S had irregular dodecahedra morphology. As a consequence, the morphology of the particles that is linked to the exposed facets showed selectivity in the type of organic substrate that is photodegraded at the surface of the photocatalyst [27]. Also, the larger surface area provides more active sites to absorb the dyes, and facilitates the separation of electron-hole pairs during the photo-chemical reaction, resulting in the superior photocatalytic activity.

Conclusion

In this study, a series of Ag_3PO_4 photocatalyst was prepared by three simple methods as precipitation liquid-liquid or mechanical homogenization of powder precursors solid-solid and by a novel method liquid-solid, using $(\text{NH}_4)_2\text{HPO}_4$ and AgNO_3 as precursors and at room temperature without any surfactant adding. The preparation methods can influence the morphology, particle size, and photocatalytic activity of the synthesized Ag_3PO_4 catalysts. Ag_3PO_4 synthesized by the novel method, which exhibited a nanorod and irregular polyhedra morphology, showed best photocatalytic activity. This photocatalyst could decolorize cationic and anionic dyes as OM, MB and CR.

References

1. J.L. Regnery, J. Barringer, A.D. Wing, C. Hoppe-Jones, J. Teerlink, J.E. Drewes, *Chemosphere* 127(2015) 136.
2. D.J. Lapworth, N. Baran, M.E. Stuart, R.S. Ward, *Environ. Pollut.* 163 (2012) 287-303.
3. Kubacka, A., Fernández-García, M., Colón, G, *Chem. Rev.* 112 (2012) 1555-1614.
4. S. Leong, A. Razmjou, K. Wang, K. Hapgood, X. Zhang, H. Wang, *J. Membr. Sci.* 472 (2014) 167-184.
5. S. K. Joung, T. Amemiya, M. Murabayashi, K. Itoh, *Chem. Eur. J.* 12 (2006) 5526.
6. Z. Yi, J. Ye, N. Kikugawa, T. Kako, S. Ouyang, H. Stuart-Williams, H. Yang, J. Cao, W. Luo, Z. Li, Y. Liu, R.L. Withers, *Nat. Mater.* 9 (2010) 559-564.
7. Ma, X.; Lu, B.; Li, D.; Shi, R.; Pan, C.; Zhu, Y, *J. Phys. Chem. C* : 115 (2011) 4680-4687.
8. M.Q. Wen, T. Xiong, Z.G. Zhang, W. Wei, X.T. Tang, F. Dong, *Opt. Express* 24 (2016) 258178.
9. J. Ma, J. Zou, L. Li, C. Yao, T. Zhang, D. Li, *Appl. Catal. B* 134-135 (2013) 1-6.
10. S.M. Hosseinpour-Mashkani, A. Sobhani-Nasab, *J. Mat. Sci. Mater. Electron.* 28 (2017) 4345-4350.
11. Jianfeng Gou, Qiuling Ma, Yuqi Cui, Xiaoyong Deng, Huixuan Zhang, Xiuwen Cheng, Xiaoli Li, Mingzheng Xie, Qingfeng Cheng, Huiling Liu, *Journal of Industrial and Engineering Chemistry* 49 (2017) 112-121.
12. H. Hu, Z. Jiao, H. Yu, G. Lu, J. Ye, Y. Bi, *J. Mater. Chem. A* 1 (2013) 2387-2390.
13. Z.-M. Yang, Y.-Y. Liu, L. Xu, G.-F. Huang, W.-Q. Huang, *Mater. Lett.* 133 (2014) 139-142.
14. K. Wang, J. Xu, X. Hua, N. Li, M. Chen, F. Teng, Y. Zhu, W, *J. Mol. Catal. A* 393 (2014) 302-308.
15. L. Dong, P. Wang, S. Wang, P. Lei, Y. Wang, *Mater. Lett.* 134 (2014) 158-161.
16. X. Guo, C. Chen, S. Yin, L. Huang, W. Qin, *J. Alloy. Compd.* 619 (2015) 293-297.
17. Y. Bi, H. Hu, S. Ouyang, G. Lu, J. Cao, J. Ye, *Chem. Commun.* 48 (2012) 3748-3750.
18. Q.H. Zhang, L. Gao, J.K. Guo, *Appl. Catal. B: Environ.* 26 (2000) 207.
19. B. Chafik El Idrissi, K. Yamni, A. Yacoubi, A. Massit, *IOSR-JAC.* 7, Issue 5 Ver. III(2014) 107-112.
20. Y. Li, W. Xie, X. Hu, G. Shen, X. Zhou, Y. Xiang, X. Zhao, P. Fang, *Langmuir* 26 (2010) 591-597.
21. M. Qamar, R.B. Elsayed, K.R. Alhooshani, M.I. Ahmed, D.W. Bahnemann, *Catal. Commun.* 58 (2015) 34-39.
22. X. Ma, H. Li, Y. Wang, H. Li, B. Liu, S. Yin, T. Sato, *Appl. Catal. B-Environ.* 158-159 (2014), 314-320.
23. Lin Luo, Yuanzhi Li, Jingtao Hou, Yi Yang, *Applied Surface Science* 319 (2014) 332-338.
24. R. Li, X. Song, Y. Huang, Y. Fang, M. Jia, W. Ma, *J. Mol. Catal. A* 421 (2016) 57-65.
25. J. Jiang, K. Zhao, X. Xiao, L. Zhang, *J. Am. Chem. Soc.* 134 (2012) 4473-4476.
26. H. Narayan, H. Alemu, L. Macheli, M. Sekota, M. Thakurdesai, T.G. Rao, Bull, *Mater. Sci.* 32 (2009) 499-506.
27. X. Chen, Y. Dai, X. Wang, *J. Alloy. Compd.* 649 : A review (2015) 910-932.

(2017) ; <http://www.jmaterenvironsci.com>